Measurement Informed Models and Digital Twins for Optical Fiber Communication Systems

Md. Saifuddin Faruk, *Senior Member, IEEE* and Seb J. Savory, *Fellow, IEEE*, *Fellow, Optica*

[Invited Tutorial]

***Abstract*—Digital coherent transceivers have developed to the stage that they can monitor the physical state of an optical network and thus are capable of generating data to build measurement-informed physical layer models. After reviewing the measurement capabilities of coherent transceivers, we discuss different modeling approaches including physics-based models, data-driven models as well as hybrid models that incorporate elements of both physics-based and data-driven models. Having reviewed both the measurement capabilities and the modeling methodologies, the salient features of building digital twins based on measurement informed models for optical fiber communication systems are discussed.**

***Index Terms*—** Digital coherent receiver, optical communication systems, digital signal processing, digital twins.

I. INTRODUCTION

COHERENT transceivers are capable of performing physical layer measurements on any optical path that connects two transceivers. This in turn enables the inference of the physical parameters of both the fiber (*e.g.* attenuation, dispersion, nonlinear coefficient) and the associated optical amplifier (*e.g.* gain spectra, noise figure, saturated noise power). Since the advent of the digital coherent transceiver, there have been numerous studies regarding the efficacy of a coherent transceiver to measure different system parameters and impairments, including the spectrum of received signal [1], IQ imbalance [2], chromatic dispersion [3], channel parameters [4], transceiver skew [5, 6], and received signal-to-noise ratio (SNR) [7, 8, 9]. A recently investigated technique, digital longitudinal monitoring, shows promise as a very powerful technique for amplified systems, ranging from core networks to submarine links [10, 11]. Using cooperation between transceivers across a network it may be possible to estimate localized effects including an individual optical amplifier noise spectrum as well as localized filtering due to a reconfigurable optical add-drop multiplexer (ROADM). As such, we have reached a point whereby digital coherent transceivers can not only characterize themselves but can also build up a picture of the whole optical network infrastructure.

The resulting measurement data allow us to create the physical layer model. There are two basic approaches of modeling based on data: the physics-based model with unknown parameters extracted from measurement data and the data-driven model based on purely data without any underpinning physics [12]. In addition, there is a hybrid modeling approach that combines physics-based modeling with high reliability and interpretability and data-driven modeling for correcting any residual error for unobserved or neglected physics [13].

With such advancement in metrology and measurement informed modeling, we can construct a '*digital twin*' which can be considered as a digital mirroring of a physical system with automatic data/information exchange between them [14]. Though the concept of digital twins started in the aerospace and manufacturing industries, recently its application for optical fiber communication systems has attracted significant attention [15, 16]. Digital twins can be applied in design, operation and future change prediction in optical systems and networks. Applications already demonstrated using digital twins include soft-failure management [17], quality of transmission (QoT) estimation and prediction [18] and signal power spectrum optimization [19]. Different software tools have also been tested as digital twins, for example, the open-source project GNPy [20], a time domain twin named OCATA [21], and a network automation framework called AI-Light [22].

As an extension of an invited tutorial talk presented at the Optical Fiber Communication Conference and Exhibition (OFC) 2023 [23], in this paper, first, we provide the concept of digital coherent transceivers and their measurement capabilities in detail. Then the physical layer modeling approaches from the measurement information are discussed. Such monitoring and modeling allow us to build digital twins for optical communication systems and networks [24]. Thereafter, we discuss the basic concepts and requirements for digital twins and then provide a literature review of recent works on digital twins in the field of optical communications.

This paragraph of the first footnote will contain the date on which you submitted your paper for review, which is populated by IEEE.

This work was supported by the EPSRC through the TRANSNET project (EP/R035342/1).

M. S. Faruk and Seb J. Savory are with the Electrical Engineering Division, Department of Engineering, University of Cambridge, Cambridge CB3 0FA, UK (e-mail: msf35@cam.ac.uk, sjs1001@cam.ac.uk).

This article generated no new data. All data underlying this study are cited in the references.

Color versions of one or more of the figures in this article are available online at http://ieeexplore.ieee.org

Finally, we conclude after discussing some of the open research challenges in this field.

II. Measurement Capability of Digital Coherent Transceivers

The widely deployed digital coherent receiver illustrated in Fig. 1, is both phase and polarization diverse, thereby able to linearly detect an incoming optical signal [25]. Using this receiver architecture, the entire electrical field associated with the optical signal within the bandwidth of the receiver is mapped into the electrical domain. Having linearly mapped the optical field into the electrical domain, it is then converted to the digital domain via analog-to-digital converters (ADCs) and processed with digital signal processing (DSP) to recover the information.

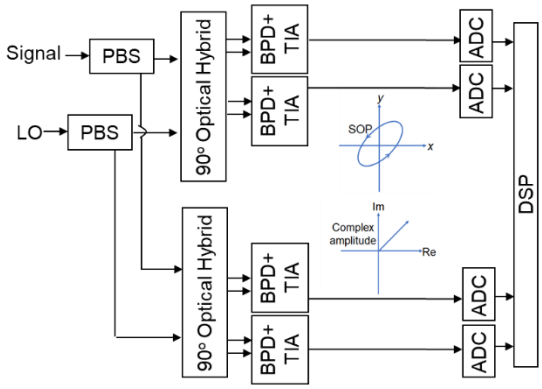

Fig. 1. Schematic standard dual-polarization digital coherent receiver. (LO: local oscillator, PBS: polarization-beam-splitter, BPD: balanced photodiode, TIA: transimpedance amplifier, ADC: analog-to-digital converter, DSP: digital signal processing).

The typical DSP chain in such a receiver includes compensation of IQ imbalance, equalization of static impairments such as chromatic dispersion (or mitigation of fiber nonlinearities), adaptive equalization of time-varying impairments, frequency offset estimation, carrier recovery, symbol estimation and decoding as summarized in Fig. 2 [26].

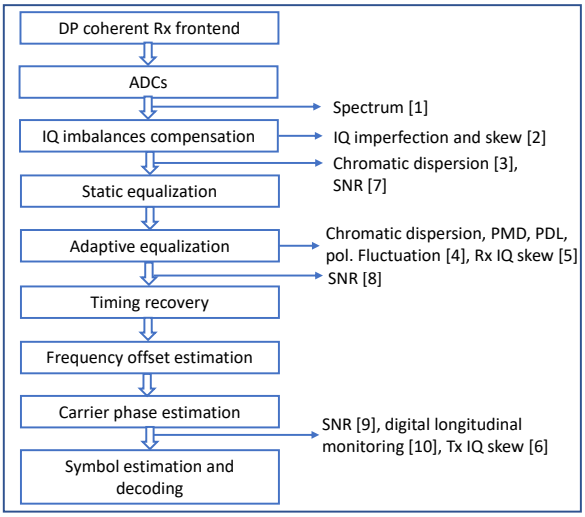

Fig. 2. Typical DSP chain in a coherent receiver and list of different sensing/monitoring positions with an exemplary reference in the DSP flow.

Provided that the full-field information is captured by the coherent receiver, the DSP can be used as a powerful tool to measure different physical layer parameters. The parameters that can be measured at different DSP stages are also illustrated in Fig. 2. Herein, we provide the underlying theory of such measurement capabilities in detail.

A. Optical Spectrum Sensing

The inherent frequency selectivity property of coherent receivers enables wideband spectral sensing [1]. The transmission frequency of the samples received by the coherent receiver is determined by the local oscillator (LO). Therefore, transforming the samples from the time domain to the frequency domain will provide a 'slice' of bandwidth equivalent to the sampling speed of the ADCs centered on the LO's frequency. By tuning the LO to a frequency grid at regular intervals and sampling at each of these grid points, a wideband spectral estimation using a receiver can be realized. These slices can then be digitally stitched together to form an estimation as wide as the LO can tune. An example of spectrum estimation of full C-band is shown in Fig. 3 with eighty-eight 35-Gbaud PM-QPSK channels [27].

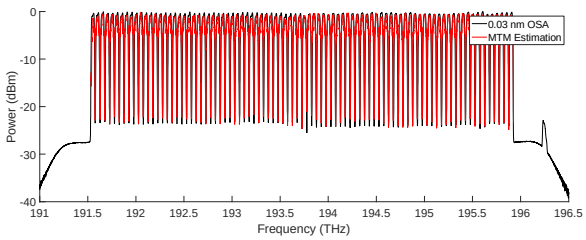

Fig. 3. Measured spectrum over C-band using the coherent receiver. From ref. [27].

Using a single coherent receiver for wideband spectrum estimation as in [27] , has the limitation that the receiver cannot be used as a part of traffic carrying channel since LO tuning is required. While this indicates what might be possible with co-operation between transceivers, when capturing the spectrum of a single-channel it enables impairments from tight filtering at ROADMs to be mitigated [28] and soft-failure detection and identification [29]. Optical channel monitoring capabilities in an elastic optical network using SDN-based spectrum monitoring have also been demonstrated [30].

B. IQ Imbalance Estimation

The receiver-side IQ phase imbalance results from imperfections in the 90° hybrid and IQ gain mismatch is induced by imperfections in balanced photodiodes and trans-impedance amplifiers used in a coherent receiver as shown in Fig.1. In addition, timing mismatch between the IQ ports may be caused by the difference in the physical path length of the circuit trace, which is known as the IQ delay skew.

The IQ gain and phase mismatch can be compensated and monitored using the Gram-Schmidt orthogonalization procedure (GSOP) [2]. For a particular polarization channel, the IQ gain mismatch level is estimated directly from real and

imaginary parts of the incoming signals using the normalization of power, and the phase mismatch level is estimated from their correlation coefficient. If we consider that the angle between the I and Q component is $\pi/2-\theta$ instead of $\pi/2$ as shown in Fig. 4, the received signal r_I and r_Q can be written as, $r_I = t_1$ and $r_Q = t_2\cos\theta - t_1\sin\theta$, where t_1 and t_2 are transmitted signals with zero mean and unit variance. Then, the phase imperfection can be estimated by cross-correlating r_I and r_Q as

$$\hat{\theta} = \sin^{-1}\left(\frac{\langle r_I r_Q\rangle}{\sqrt{\langle r_I^2\rangle\langle r_Q^2\rangle}}\right) \quad (1)$$

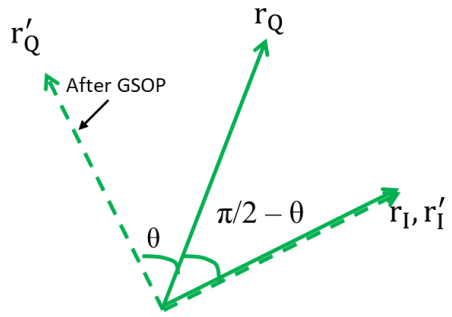

Fig. 4. Visualization of non-orthogonality in a coherent receiver.

A similar approach can be used to detect skew τ considering that skew is compensated at maxima of $\langle r_1(t)r_2(t+\tau)\rangle$.

C. Chromatic Dispersion Estimation

The chromatic dispersion can be explained as an all-pass filter in the frequency domain and expressed as [31]:

$$H_{CD}(z,\omega) = \exp\left(j\frac{\lambda^2\omega^2}{4\pi c}Dz\right) \quad (2)$$

where, z is the propagation distance, ω is the angular frequency, λ is the wavelength, c is the speed of light and D is the chromatic dispersion coefficient.

There are several blind algorithms to estimate the accumulated chromatic dispersion, Dz, which can be broadly classified as the scanning method and the single-step method. In the case of the scanning method, the received signal is filtered with a chromatic dispersion compensating digital filter having a transfer function of $1/H_{CD}(z,\omega)$ over a range of preset chromatic dispersion such as $0{:}\,\delta(Dz){:}\,(Dz)_{max}$, where $\delta(Dz)$ is scanning resolution and $(Dz)_{max}$ is estimation range. Then, a cost function from the equalized signal is utilized to select the estimated value. Several cost functions are investigated such as based on the constant modulus algorithm (CMA) [32], signal peak-to-average power ratio (PAPR) [33], modified discrete circular auto-correlation in the frequency domain [34], etc. Generally, for a scan-based algorithm, a smaller scanning step size is required for more accurate estimation, which in turn increases the computational burden. A way to reduce the scanning number is to do a coarse estimation with a large step size and then a fine scanning around the estimated value in the first stage.

In contrast, signal power autocorrelation can be used to estimate the chromatic dispersion in one step [3]. The autocorrelation function of the received signal power has two components: the first component is related to the power of individual symbols and the second component is related to the interference between symbols. For a sufficiently high chromatic dispersion, the first term is a constant and the second term gives a peak value, whose position is related to the accumulated chromatic dispersion. This method assumes that the input signal is a Gaussian pulse and thus provides an inaccurate result for a small accumulated dispersion. To overcome this problem, a large known chromatic dispersion can be artificially added before the estimation and then subtracted after the estimation to predict the correct value [35].

D. Multi-Parameters Estimation from the Adaptive Equalizer

Considering the usual arrangement of 2×2 complex FIR filters as shown in Fig. 5 to correct for dynamic channel impairments [31], the filter tap coefficients of the equalizer after the convergence represent the inverse impulse response of the channel, thus enabling monitoring of the channel parameters.

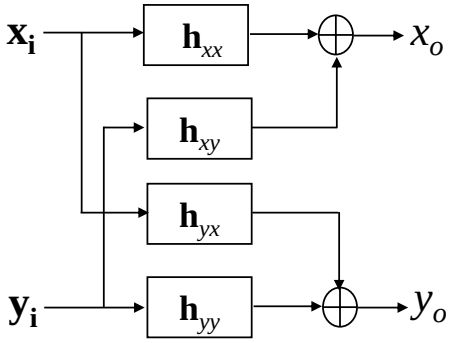

Fig. 5. Configuration of 2×2 MIMO equalizer used to compensate for the dynamic channel impairments. $\mathbf{x}_i$ and $\mathbf{y}_i$ are the inputs and x_o and y_o are the outputs of the equalizer for *x*- and *y*- polarization, respectively.

A two-by-two monitoring matrix $\mathbf{M}(\omega)$ can be constructed with four elements corresponding to the transfer function of four filters as:

$$\mathbf{M}(\omega) = \begin{bmatrix}\mathbf{H_{xx}}(\omega) & \mathbf{H_{xy}}(\omega)\\ \mathbf{H_{yx}}(\omega) & \mathbf{H_{yy}}(\omega)\end{bmatrix}^{-1} \approx \mathbf{H}_{fiber}(\omega), \quad (3)$$

where, $\mathbf{H}_{ij}(\omega) = \text{DFT}(\mathbf{h_{ij}})$; *ij*=*xx*, *xy*, *yx* or *yy*, DFT is discrete Fourier transform and ω is the angular frequency of the optical carrier. $\mathbf{H}_{fiber}(\omega)$ is the transfer function of the fiber channel which can be modeled as the concatenation of chromatic dispersion, differential group delay (DGD), polarization-dependent loss (PDL) and polarization rotation elements as:

$$\mathbf{H}_{fiber}(\omega) = H_{CD}(\omega)\times\mathbf{U}(\omega)\times\mathbf{K}\times\mathbf{J}, \quad (4)$$

Chromatic dispersion is a scalar element given by Eq. (2), with DGD, PDL and polarization rotations elements

represented by **U**(ω), **K** and **J**, respectively, in the matrix forms given by [36]:

$$\mathbf{U}(\omega) = \mathbf{R}_1^{-1}\begin{bmatrix} e^{\frac{j\omega\Delta\tau}{2}} & 0 \\ 0 & e^{-\frac{j\omega\Delta\tau}{2}} \end{bmatrix}\mathbf{R}_1^{-1},$$

$$\mathbf{K} = \mathbf{R}_2^{-1}\begin{bmatrix} \sqrt{\Gamma_{max}} & 0 \\ 0 & \sqrt{\Gamma_{max}} \end{bmatrix}\mathbf{R}_2^{-1},$$

$$\mathbf{J} = \begin{bmatrix} \cos\theta & \sin\theta\, e^{-j\phi} \\ -\sin\theta\, e^{j\phi} & \cos\theta \end{bmatrix},$$

where, $\mathbf{R}_1$ is a unitary matrix converting two PSPs into the *x*- and *y*-polarization, $\Delta\tau$ is the DGD, $\mathbf{R}_2$ is another unitary matrix converting the eigenmodes for PDL into the *x*- and *y*-polarization, Γ_{max} and Γ_{max} are the maximum and minimum transmission efficiency, respectively, and 2θ and ϕ are the azimuth and elevation rotation angles between two polarization states, respectively.

The challenge is to separate all these channel parameters from a single matrix $\mathbf{M}(\omega)$. Several algorithms have been investigated for this purpose [36, 37, 4] which are based on the characteristics of different channel parameters. The H_{CD} is a scalar function, **U** is a frequency-dependent unitary matrix, **K** is a Hermitian matrix and **J** is another unitary matrix whose elements are independent of angular frequency. As an example, the four parameters can be estimated as follows:

Residual chromatic dispersion can be estimated by quadratic fitting to the unwrapped phase of the determinant of the monitoring matrix, $|\mathbf{M}(\omega)|$.

The DGD can be estimated by measuring the monitoring matrix at two frequencies ω and $\omega + \Delta\omega$ and then calculating the eigenvalues ρ_1 and ρ_2 of the matrix $\mathbf{M}(\omega+\Delta\omega)\mathbf{M}(\omega)^{-1}$. The DGD, Δτ is given as $\Delta\tau = \frac{\arg(\rho_1/\rho_2)}{\Delta\omega}$.

The PDL is estimated from the eigenvalues Γ_1 and Γ_2 of matrix $\mathbf{M}(\omega)^{\mathrm{H}}\mathbf{M}(\omega)$ as $10\log_{10}(\Gamma_1/\Gamma_2)$, where superscript $(.)^{\mathrm{H}}$ is the Hermitian operator.

Finally, to estimate the change in the polarization state, the monitoring matrix at DC can be used. If we consider an input $\mathbf{J_{x,in}} = [1, 0]^{\mathrm{T}}$ with the horizontal polarization, the average output (at DC) will be $\mathbf{J_{x,out}} = [E_x, E_y]^T = [H_{xx}(0), H_{xy}(0)]^T$. This allows the Stokes parameter to be estimated as [38]:

$$\mathbf{S} = \begin{bmatrix} S_0 \\ S_1 \\ S_2 \\ S_3 \end{bmatrix} = \begin{bmatrix} |E_x|^2 + |E_y|^2 \\ |E_x|^2 - |E_y|^2 \\ E_x E_y^* + E_x^* E_y \\ jE_x E_y^* - jE_x^* E_y \end{bmatrix}. \quad (5)$$

Measuring the Stokes parameter at successive time instances enables the estimation of changes in the polarization state. Recently several exciting new applications enabled by such polarization fluctuation monitoring have been demonstrated. For example, in [39], the link monitoring and active detection of link tampering were demonstrated in the metro network by sensing the SOP in an FPGA-based real-time coherent transceiver prototype. A similar approach was used to monitor environmental perturbations affecting the fiber link from the field trail data measured on cabled multi-core-fibers (MCF) with nominally uncoupled cores deployed in the city of L'Aquila, Italy [40]. Measuring the mechanical stress on an optical fiber and consequently proactive fiber damage detection was demonstrated in [41]. The SOP monitoring from the filter taps of regular optical telecommunication channels was used to successfully sense the seismic and water waves over a 10,000-kilometer-long submarine cable (Curie cable) connecting Los Angeles and Valparaiso Chile [42].

To compensate for the receiver IQ skew, a complex-valued 4×2 MIMO as detailed in Fig. 6 can be used as an alternative to 2×2 MIMO. Such equalizer thus enables the estimation of IQ skew from the filter taps after convergence. The delay is noticeable in the frequency domain as a linear variation of the phase and it is a function of the frequency. Therefore, to estimate the skew, first, the differential phases are calculated from the frequency response of the converged filter tap coefficient as [5]:

$$\varphi_x(f) = \arg\{\mathbf{H}_{x_r,x} \cdot \mathbf{H}_{x_i,x}^* + \mathbf{H}_{x_r,y} \cdot \mathbf{H}_{x_i,y}^*\}, \quad (6)$$

$$\varphi_y(f) = \arg\{\mathbf{H}_{y_r,x} \cdot \mathbf{H}_{y_i,x}^* + \mathbf{H}_{y_r,y} \cdot \mathbf{H}_{y_i,y}^*\}, \quad (7)$$

where, $\mathbf{H}_{\_,\_} = \mathrm{DFT}(\mathbf{h}_{\_,\_})$ and superscript $(.)^*$ is the conjugate operation. The skew can be inferred from this phase, for example, by exploiting a linear regression of the phase to find the slope, which is proportional to the skew [5].

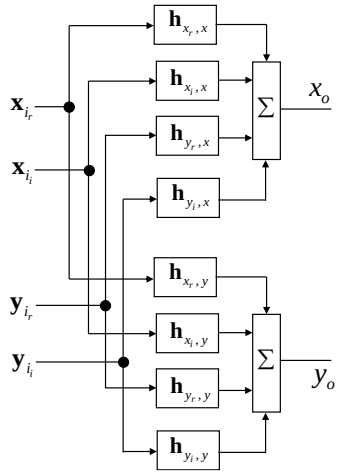

Fig. 6. Configuration of 2×4 MIMO equalizer to incorporate compensation and estimation of receiver-side IQ skew.

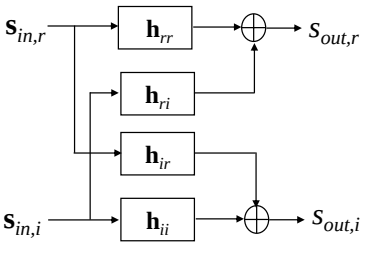

Fig. 7. Configuration of 4×4 real-valued MIMO equalizer to allow compensation and estimation of transmitter-side IQ imbalance.

After the carrier phase recovery, for each polarization channel, another 4×4 real-valued MIMO equalizer as shown in Fig. 7 can be used to compensate and monitor the transmitter side IQ imbalance [6]. The gain imbalance is estimated from direct tap coefficients as:

$$\hat{g}_{\iota,dB} = 20\log_{10}\left(\frac{\sum \mathbf{h}_{rr}}{\sum \mathbf{h}_{ii}}\right) \quad (8)$$

The phase imbalance is calculated from direct and crossed tap coefficients as:

$$\hat{\theta}_{deg} = 2\sin^{-1}\left(\frac{\sum \mathbf{h}_{ir}}{\sum \mathbf{h}_{rr}}\right)\frac{180}{\pi} = 2\sin^{-1}\left(\frac{\sum \mathbf{h}_{ri}}{\sum \mathbf{h}_{ii}}\right)\frac{180}{\pi} \quad (9)$$

Finally, the frequency-dependent skew is estimated from the group-delay difference of the direct tap coefficient as:

$$\hat{\tau}(\omega) = \frac{d\boldsymbol{H}_{rr}(\omega)}{d\omega}\boldsymbol{H}_{rr}(\omega)^{-1} - \frac{d\boldsymbol{H}_{ii}(\omega)}{d\omega}\boldsymbol{H}_{ii}(\omega)^{-1} \quad (10)$$

E. SNR Monitoring

SNR, the ratio of signal power to noise power, is a generic metric used to measure transmission performance in telecommunication engineering [43]. In a coherent receiver, when the SNR is evaluated in the digital domain before FEC to include both linear and nonlinear noise, it is often called effective SNR (ESNR) or generalized SNR (GSNR) [44]. In contrast, the optical SNR (OSNR), measured in the optical domain before the coherent receiver, considers amplified spontaneous emission (ASE) noise only for an optically amplified system as defined in the IEC-61280-2-9 standard. Sometimes the term generalized OSNR (GOSNR) is also used to describe optical GSNR to include the nonlinear noise [45].

There are several stages in the DSP chain where the SNR can be estimated as shown in Fig. 2. It can be measured straight after the digitization of ADCs raw data, after the adaptive equalization with the equalized signal or at the symbol estimation and decoding stage.

First, consider the SNR estimation straight after the digitization. It can be done by loading a spectral perturbation at the transmitter, for example, a simple dual-notch perturbation can be utilized for this purpose [7]. The dual-notch filter is symmetric around the carrier as illustrated in Fig. 8, where the bandwidth of the notch is BW_N and the bandwidth of the transmitted signal is BW_T. A digital coherent receiver is then used to measure the underlying noise floor segments that are spectrally stitched with contiguous noise floor spectra which enables the separation of signal and noise components in the frequency domain and thus estimation of associated signal-to-noise-distortion ratio (SNDR). This technique is simple and can be used at the start-up time. However, this method has the drawback that while using it for continuous monitoring purposes, some spectrum is sacrificed to include the notch, thereby decreasing the spectrum available for data modulation.

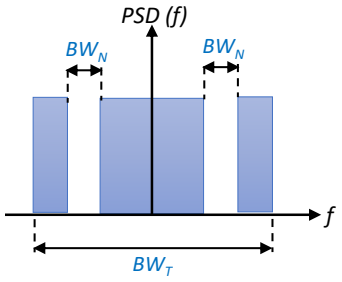

Fig. 8. Illustration of a dual-notch perturbation used to measure the SNR.

To overcome such limitation, a second approach is to estimate the SNR after the dynamic channel equalization. This technique was first demonstrated for the QPSK equalized signal after the CMA by taking the second- and fourth-order statistical moments of the equalized signal [8, 46]. Later, its extension for the *M*-QAM format is demonstrated in [47, 48], where the SNR is estimated as:

$$\mathrm{SNR}_{dB} = 10\log_{10}\left\{\frac{\sqrt{2M_2^2 - M_4}}{M_2 - \sqrt{2-k_s}\sqrt{2M_2^2 - M_4}}\right\}, \quad (11)$$

where, M_2 and M_4 are the second- and fourth-order moments of the measured equalized signal and k_s is the kurtosis of transmitted symbols which is constant for a particular modulation format. The benefit of this method is that the estimation performance is independent of transmission impairment as it is measured after equalization. It is also unaffected by phase noise even though it is estimated before carrier recovery as the method is based on amplitude noise alone. The drawback of this method is that the estimation performance is degraded with the increase of modulation order. However, techniques such as partitioning the ring of higher-order QAM constellation can be utilized to improve performance [49].

Another straightforward approach to estimate SNR is at the end of the receiver DSP chain when the signal has been recovered. At this stage, the error vector is calculated by the vector subtraction of the ideal transmitted signal and measured signal as shown in Fig. 9. Then, the error vector magnitude (EVM) which is defined as the rms value of error vectors measured from the received symbols are computed as [50]:

$$\mathrm{EVM} = \sqrt{\left\{\frac{1}{N}\sum_{n=1}^{N}|s_m(n) - s_i(n)|^2\right\}/P_0}, \quad (12)$$

where, N is the number of symbols over which the value of EVM is estimated, $s_m(n)$ is the n^{th} measured received symbol, $s_i(n)$ is n^{th} the ideal transmitted symbol and P_0 is either the maximum ideal symbol power or the average power of all symbols in the constellation. For the data-aided system, $s_i(n)$ is the known transmitted symbol whereas for a non-data-aided system, this is the decoded symbol from $s_m(n)$. Once the EVM is measured, the SNR can be calculated from the analytical formula as in [9, 51]:

$$\mathrm{EVM}=\frac{1}{k}\left[\frac{1}{\mathrm{SNR}}-\sqrt{\frac{96}{\pi(M-1)\mathrm{SNR}}}\sum_{i=1}^{\sqrt{M}-1}\gamma_i e^{\frac{3\beta_i^2\mathrm{SNR}}{2(M-1)}}+\frac{12}{(M-1)}\sum_{i=1}^{\sqrt{M}-1}\gamma_i\beta_i\mathrm{erfc}\left(\sqrt{\frac{3\beta_i^2\mathrm{SNR}}{2(M-1)}}\right)\right]^{1/2} \quad (13)$$

where, k is a modulation format dependent factor, M is the modulation order, $\gamma_i=1-i/\sqrt{M}$ and $\beta_i=2i-1$. The expression in Eq. (13) is for a non-data-aided EVM calculation and this relationship can be simplified as EVM $\approx 1/k\sqrt{\mathrm{SNR}}$ in the case of high SNR.

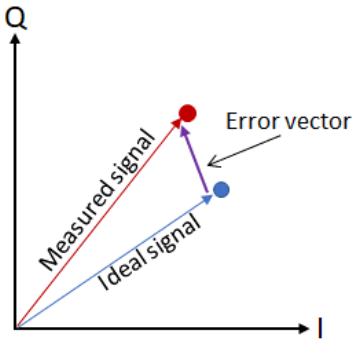

Fig. 9. Illustration of error vector definition.

The OSNR is related to SNR as $\mathrm{OSNR}=\frac{pR_s}{B_{ref}}\mathrm{SNR}$ [43]. where, p = 1 for single-polarization or 2 for dual-polarization signal, R_s is the symbol rate and B_{ref} is the reference bandwidth which is usually chosen as 0.1 nm. Note that, a further calibration factor needs to be considered for the SNR-OSNR relationship to include the impact of optical filtering from routing nodes in an optical network [52, 53].

For a polarization multiplexed system, a similar OSNR is expected on both polarization tributaries, however, this is not the case in the presence of PDL [54]. The OSNR fluctuation depends on the orientation of the polarization multiplexed data signal and the PDL element. The worst-case scenario is when the lossy axis of the PDL element is aligned to one of the polarization channels. The OSNR fluctuation associated with PDL cannot be fully compensated using receiver DSP, however, it be mitigated, for example, by controlling the SOP at the transmitter side [55].

The SNR can also be inferred from the pre-FEC BER. For example, $\mathrm{SNR}_{\mathrm{BER}}$ relates to BER for an M-QAM signal as [56]:

$$BER\cong A\,\mathrm{erfc}(\sqrt{B SNR_{BER}}) \quad (14)$$

where, erfc(·) is the complementary error function and A and B are modulation format dependent factors.

In practice, when the $\mathrm{SNR}_{\mathrm{BER}}$ is estimated in a modem, an eye-closure (EC) factor (with EC<1, depends on modem parameters such as the DSP and jitter) is multiplied with $\mathrm{SNR}_{\mathrm{BER}}$ to obtain the accurate SNR [57]. The EC can be measured by comparing the SNR measured with an optical spectral analyzer (OSA) and that from pre-FEC BER [58]. Assuming the noise is Gaussian, another performance metric, Q^2-factor can be estimated from the pre-FEC BER such that $Q^2-\mathrm{factor}\,[dB]=20\log_{10}\left(\sqrt{2}\,\mathrm{erfc}^{-1}(2\times\mathrm{BER})\right)$ [59].

Noise Segregation:

Although a receiver can measure overall SNR, it is generally composed of several elements. It is therefore useful to segregate the different elements for network design and management purposes. Assuming that the contributing noise terms are independent and Gaussian, we can sum the inverse of the SNR being the noise-to-signal ratio (NSR) from the element to obtain the overall NSR from which the total SNR can be calculated. This is a reasonable assumption for a high dispersion system and the basis of the Gaussian noise (GN) model [60]. Thus, the total SNR can be expressed as [61, 62]:

$$\mathrm{SNR}_{total}=\left\{\frac{1}{\mathrm{SNR}_{LIN}}+\frac{1}{\mathrm{SNR}_{NLI}}+\frac{1}{\mathrm{SNR}_0}\right\}^{-1}, \quad (15)$$

where, SNR_{LIN} corresponds to the linear term which is coming from the ASE noise of the amplifiers, SNR_{NLI} is the nonlinear term stemming from the fiber Kerr linearity, and SNR_0 is the modem-dependent term including transceiver noise, quantization noise, implementation penalty from DSP, etc.

One means of noise segregation is to exploit a key property of each noise term, for example, SNR_0 does not change with propagation distance in contrast to the other two noise terms SNR_{NLI}, SNR_{LIN} which are distance-dependent. Likewise, unlike SNR_{NLI}, SNR_{LIN} is independent of launch power. Thus, we can rewrite Eq.(15) as [63]:

$$\mathrm{SNR}_{total}(k)=\left\{\frac{ASE_0 k}{P_{sig}}+\gamma^2 f(k)P_{sig}^2+\frac{1}{\mathrm{SNR}_0}\right\}^{-1}, \quad (16)$$

where, k is the number of spans, ASE_0 is the average ASE noise power per span, P_{sig} is the signal power, γ is the nonlinear coefficient, and $f(k)$ is a pre-calculated factor by the EGN model [64]. Now, the link can be abstracted using the three global parameters (total ASE noise, $ASE(k)=ASE_0 k$, NLI coefficient, $\eta(k)=\gamma^2 f(\mathrm{k})$ and SNR_0) extracted from the experimental measurements using Eq. (16). Such an approach is experimentally verified in [63].

Another approach for noise segregation is decomposing the noise variance for each symbol into its normal, **n**, and tangential, **t**, components. For an M-QAM signal, it is possible to calculate the average of each constellation ring resulting N_v and T_v (v is the ring index), respectively, and these metrics correspond to a classification of the noise components of the EVM metric which is directly related to SNR. An example for 16-QAM is shown in Fig. 10 for which SNR is calculated as [65]:

$$SNR_{16-QAM}=\frac{16}{4N_1+8N_2+4N_3+4T_1+8T+4T_3}. \quad (17)$$

To segregate the SNR_{LIN} and SNR_{NLI}, machine learning (ML) based modeling can be used. For example, in [65], a neural network (NN) was used for SNR decomposition with

input features as N_v, T_v, number of WDM channels and accumulated chromatic dispersion while the output label of NN was SNR_{LIN} and SNR_{NLI}.

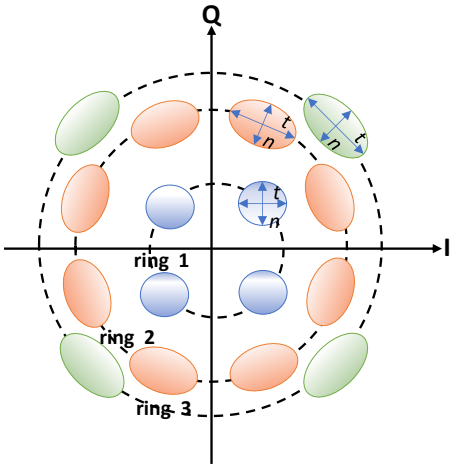

Fig. 10. Illustration of normal and tangential components for 16-QAM modulation format.

There are several other approaches for noise segregation such as the use of amplitude noise correlation across neighboring symbols [66], amplitude modulation pilot tone [67], ML-based approach using amplitude noise covariance and phase noise covariance [68, 69], etc.

F. Digital Longitudinal Monitoring

The coherent receiver-based monitoring discussed so far can only estimate the cumulative values along the entire fiber link. However, it would be significantly useful if the receiver provides not only the cumulative values but also the variation of such parameters as a function of distance.

The monitoring of fiber longitudinal parameters includes fiber link power (or loss) profile, chromatic dispersion maps, individual characteristics of link components like amplifier gain spectrum, the response of the optical filter and so on. Usually, analog measuring instruments like optical time-domain reflectometers (OTDR) and OSA are used for such monitoring purposes. Recently, as an alternative, monitoring of such parameters using the DSP in the coherent receiver has been demonstrated and termed as digital longitudinal monitoring (DLM) [70].

Early work in this field demonstrated measurements of the wavelength-dependent power profile and gain evolution over ten 80-km span links by sending a pump and a probe/pilot signal at two different wavelengths and exploiting their nonlinear interaction [71]. Albeit the technique provided good accuracy with a maximum error of 0.3 dB, it required two ITU channels for measurement. Therefore, attention turns to the methods that enable measurement from a data traffic-carrying channel.

First, consider the case of longitudinal power profile monitoring. The power variations due to fiber losses and amplifications along a link are governed only by $\gamma'(z)$ in the nonlinear Schrödinger equation:

$$\frac{\partial A}{\partial z} = j\frac{\beta_2}{2}\frac{\partial^2}{\partial t^2}A - j\gamma'(z)|A|^2A, \qquad (18)$$

where, $\gamma'(z) = \gamma P(0)\exp\left(-\int_0^z \alpha(z')dz'\right)$. Also, A, β_2, γ, α and z are propagated optical signal, group-velocity dispersion parameter, nonlinear coefficient, loss coefficient and propagation distance, respectively. To estimate the longitudinal power profile, $\gamma'(z)$, which carries the power variation information is estimated by comparing the received signal, A_{Rx} $[L]$ and virtually propagated reference signal A_{ref} $[L]$ for the link length L. The estimation of $\gamma'(z)$, denoted by $\widehat{\gamma'}(z)$ can be obtained using either correlation methods (CM) [72, 73, 11] or minimum mean square error (MMSE) [70, 74, 75] as shown in Fig. 11. The CMs are more robust to noise and distortion than the MMSE methods. However, unlike the CMs, the MMSE methods have the benefit that the estimation performance is independent of modulation formats. Since the longitudinal power profile monitoring is based on fiber nonlinearity estimation, it performs well with high launch power. The estimation performance is expected to deteriorate with a decreasing launch power. Further investigation is required on the estimation performance for the system operating on linear or weakly nonlinear regions.

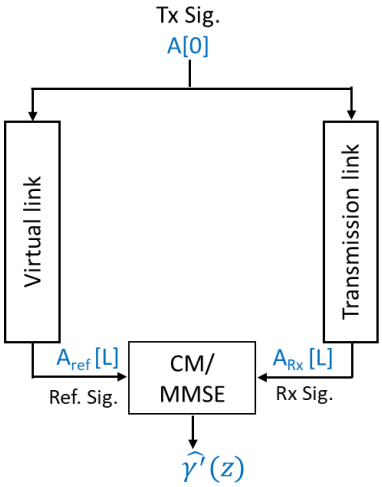

Fig. 11. Schematic of the principle of longitudinal power profile estimation models.

Obtaining longitudinal power profile estimation in each channel of a WDM system enables a wavelength-dependent visualization of the power profile along the link. This in turn allows estimation of the optical amplifier gain spectrum. It also enables the detection of amplification-related anomalies, such as gain tilt and narrowband gain compression. The applicability of this method has been demonstrated for both EDFA [76] and Raman amplifiers [77].

The other applications of digital longitudinal monitoring include location-resolved PDL monitoring in a multi-span transmission link [78], extraction of chromatic dispersion profile and optical filter (*e.g.* WSS) response [70].

III. Measurement-Based Physical Layer Model

Most models we use are informed by measurements and the model in turn informs the measurements to be taken for the model. For a physical layer model, the properties or

parameters are informed by physical measurements. From experimentally measuring parameters we can feed them into a theoretical model or equally, we can generate a pure data-driven model without any underpinning physics. Generally, there is also a link between our physical understanding of the entity to be modeled and the model as shown in Fig. 12. This allows us to get an understanding of what is happening in the physical entities and the model. Now, this could be a model based on our understanding of the physics of the problem. It also could incorporate a-priori knowledge of what model parameters might be reasonable either in terms of value or range. So, if the model gives a prediction that is outside the range, we understand there is something wrong with our measurement. Furthermore, we want to interpret the model to check our understanding.

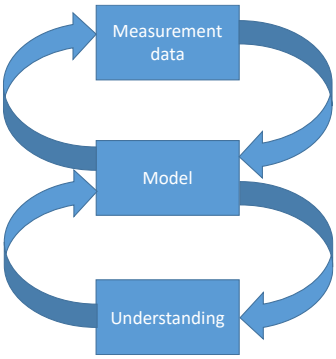

Fig. 12. The link between the physical understanding of the entity to be modeled, the model and the measurement data.

While not explicit there is a loss function that informs this feedback. Generally, we are looking for the simplest model that can explain the measurement data within the accuracy of the measurements. Measurements always have uncertainty associated with them. Physical layer models need to take this into account. There are several approaches to deal with this. For example, the statistical distribution of the parameters can be included into the model. We can also limit the complexity of the model to the minimum which gives the accuracy comparable to the accuracy of the measurements. Further, we can perform Latin hypercube sampling for the input variables to efficiently sample from the parameter space [79].

Usually, optical networks are designed with a high level of performance margin to ensure service level agreements (SLAs) throughout the system's lifetime. A significant portion of the design margin is maintained to account for the inaccuracy of performance metrology tools or physical layer parameter uncertainties over the lifespan. We can learn from the physical layer measurement data to account for such uncertainties in the performance estimation model. The overall performance uncertainties can be linked with input parameter uncertainties and consequently resulting in the minimization of the performance margin [80]. The ML approach such as based on the gradient descent method can be used to reduce the uncertainty of some input parameters for the QoT model [81]. Statistical ML approach, for example, the Gaussian process (GP) is also a powerful tool to account for the level of uncertainty associated with predictions [82]. It is quantified in an interpretable way by defining a confidence region in terms of the number of standard deviations of variation away from the predictive mean. Some of the performance estimator inaccuracies arise from the uncertainty of the fiber type used in the network. To reduce such uncertainties, fiber types for all unknown links in an optical network can be identified by monitoring accumulated chromatic dispersion over all network light paths [83]. In an open, multi-vendor system, such as open ROADM, the uncertainty of the optical characteristics of the networks is increased due to the variety of components used for the deployment. Thus, the physical layer abstraction for such a multi-vendor network is particularly important to accurately evaluate the performance metric. For an Open ROADM system, a so-called 'living network' was proposed which constantly monitors the performance of an established light path by means of collecting BER information using an active spare coherent transponder [84]. Alternatively, a dynamically configurable optical impairment model enabling physical parameters learning for accurate QoT estimation was investigated in [85]. The European project ORCHESTRA utilized a coherent transponder as a software-defined optical performance monitor and then monitoring information was analyzed to obtain accurate knowledge of the physical layer and consequently used to optimize the network to reduce overprovisioning and regulate the margin [86]. The ability of the ORCHESTRA solution to meet the fundamental requirements for margin-less operation of optical networks was also demonstrated in [87].

Classification of Modeling:

There are different approaches of modeling, from the pure physics-based white box model to the data-driven black box model as shown in Fig. 13. The hybrid model provides grey box modeling which combines both physics- and data-driven approaches.

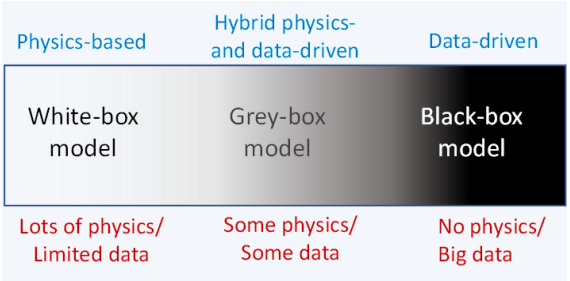

Fig. 13. Model spectrum: from physics-based white-box to data-driven black-box model.

A. Physics-Based Model

The physics-based models use a set of governing equations representing known and understood physical phenomena of the system to be modeled. All equations and parameters are known, though the model uses unknown parameters that need to be inferred from measurement data.

Generally, physics-based models are very reliable and interpretable, with the behavior typically bounded by the underpinning physics. As such, usually, the error of the model can be estimated and bounded. Also, it is less sensitive to bias.

Additionally, it is more generalizable for new systems with similar physical phenomena.

However, when creating a physics-based model, it is generally a simplification of the complete physics of the system. When the model operates in a regime where the simplification may not be valid, a residual error will occur, because, some relevant physics may be unobserved, neglected with simplifying assumptions, setting boundary conditions or uncertainties in the input parameters. Also, if the physical system significantly changes throughout its lifetime, it may behave poorly unless the models are updated to reflect the changes.

B. Data-Driven Model

Data-driven models attempt to create a model based purely on data without reference to the underpinning physics. There are no system equations or known parameters, rather the model behaviors are determined solely by measurement data used to create this. Most of the traditional ML models are data-driven black box models.

Data-driven models are very effective for problems that are too complicated to explain by pure physics. This approach includes neglected/unknown physics and thus if tuned and trained perfectly, can replicate complete physics. It also offers the benefit of continuous updates while the physical system is running and thereby adjusts for any changes that the physical system undergoes over time.

However, data-driven models are biased toward the data used to train them and thus have limited generalizability. Even with recent research focused on explainable artificial intelligence [88], it is still challenging to prove accurately what physics is modeled. Thus, purely data-driven modeling will give less confidence to use in critical applications. Additionally, only a data-driven approach generally requires a very large amount of data for training and thus can be very computationally expensive. It can also suffer from an 'overfitting' problem by learning coincidental features or noise, which will cause a well-trained model to perform poorly with new data.

C. Hybrid Physics- and Data-Driven Model

The hybrid approach of physics- and data-driven modeling, forming a grey box model, can merge the benefits of both a physics-based and data-driven approach. This approach uses some physics and some measurement data, however, requires much less data than a purely data-driven approach.

Hybrid models are a particularly desirable option for digital twin applications for several reasons. They allow for online model updates unlike physics-based models and relax the requirement of large computational power with big data for data-driven models. They also enable avoiding the uncertainty of fully data-driven models and eliminating the 'overfitting' problem of the training dataset.

There are several hybrid physics- and data-driven approaches such as physics-informed ML [89], reduced order model [90], physics-guided neural network [91], hybrid analysis and modeling [92], and so on.

Among the above different techniques, the application of physics-informed ML for optical communication has been emerging in recent years [93, 94]. Both the NN and kernel-based physics-informed methods are demonstrated. For example, physics-informed NN was used to solve the nonlinear Schrödinger equation (NLSE) in an optical fiber to estimate the fiber parameters [95]. The physics-informed GP regression method was used for the same purpose [96] as well as for the SNR estimation [82].

There are three key components of ML-based problem-solving: data, model architecture and optimization. Each of these can be integrated with physics-based knowledge to form physics-informed ML [97]. A typical way for embedding physics in data is to generate training data in simulation with the desired physics knowledge. A NN initially trained with such data will deliver a good approximation of the physical system. Designing computation graphs that mimic the behavior of physics knowledge is an example of physics-informed NN architecture design. Finally, in the optimization process, the prior physics-based knowledge can be directly incorporated into the loss function in the training process which tends to converge the model close to the possible physics-based solution.

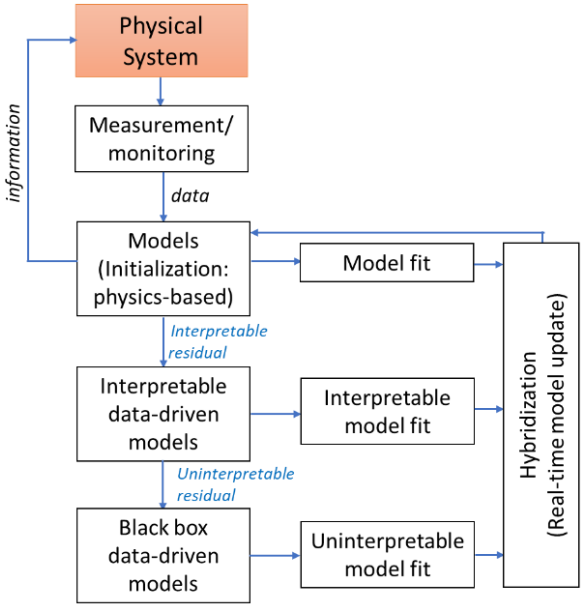

Fig. 14. The concept of hybrid analysis and modeling: the model starts with a pure physics-based model and continuously updates using knowledge generated from the data.

Another promising hybrid physics and data-driven approach is hybrid analysis and modeling which emerges in digital twin applications [92, 13]. The concept of how it works is illustrated in Fig. 14. The first step of this modeling is to use a well-understood physics-based method. The uninterpretable observation at this stage can be considered as an interpretable residual. This is modeled in the second step, with an interpretable data-driven approach. An uninterpretable residual remains after the second step which is modeled using a black-box model in the third step. The remaining residual after the third stage can be considered as random noise. With the availability of new data, these steps are continuously looped as shown in Fig. 14.

All these three steps of hybrid modeling provide a better understanding of data and thus provide an improved model

that overcomes the drawbacks of either pure physics or a pure data-driven approach. Given that most of the models used in optical communication are based on well-understood physics, the first step provides high confidence to use. Using the interpretable data-driven approach in the second stage to cope with interpretable residual (which mostly accounted for the perturbation of the model used in the first stage) again provides high confidence to use. Therefore, hybrid analysis and modeling provide a good measurement-based physical layer model which is the basis of digital twins.

IV. Brief Overview of Digital Twins

A. Definitions of Digital Twins

Though the concept of 'digital twin' has been used for nearly the last few decades, it continues to evolve as it opens out to new applications and use cases. As a result, a variety of definitions are available in the literature. Some of the key definitions are provided here.

Digital twins were imagined as '*mirror worlds*' by David Gelernter in 1991 who defined it in his book as [98]:

"They are software models of some chunk of reality, some piece of the real world going on outside your window. Oceans of information pour endlessly into the model; so much information that the model can mimic the reality's every move, moment-by-moment".

Michael Grieves, widely recognized as the father of digital twins, who initially terms it as mirror spaced model (MSM), described it as [14]:

"consists of three elements: real space, virtual space(s), and a linking mechanism, referred to as data, and information/process connection real space and virtual space(s)".

The term 'digital twin' was coined by John Vickers of the National Aeronautics and Space Administration (NASA). NASA is one of the pioneers in developing and using it, and defined it as [99]*:*

"A digital twin is an integrated multi-physics, multi-scale, probabilistic simulation of a vehicle or system that uses the best available physical models, sensor updates, fleet history, etc., to mirror the life of its flying twin".

Finally, a modern definition of digital twins referred from IBM is as follows [100]:

A digital twin is a virtual representation of an object or system that spans its lifecycle, is updated from real-time data, and uses simulation, machine learning and reasoning to help decision-making".

Several similar concepts are sometimes wrongly identified as *digital twins* [101]. Some examples are as follows:

Simulation:
Simulation is built from a physical counterpart with optional one-time data exchange from the physical system.

Digital Model:
All the data flow is done manually. Any change in the state of the physical or digital object has no direct reflection.

Digital Shadow:
Automatic data flows from the physical to the digital object. A change in the physical object can interfere with the digital, but the opposite does not occur.

On the other hand, in the case of digital twins, a fully automated data flow occurs between two objects. The changes in any object, physical or digital, directly lead to changes in the other. A summary of these different techniques is illustrated in Fig. 15.

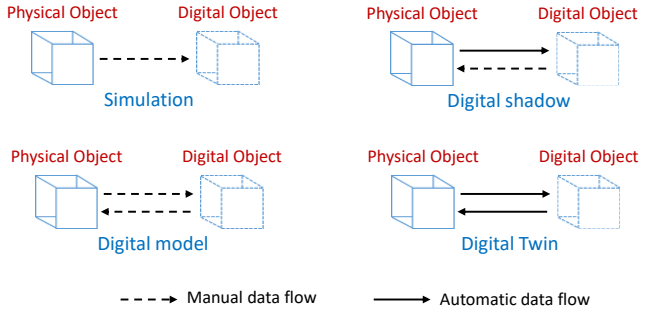

Fig. 15. Data flow characteristics between physical and digital objects for simulation, digital shadow, digital model and digital twin.

B. Types of Digital Twins

There are various types of digital twins depending on the different levels of abstraction. Some examples are as follows:

Component (or part) twins:
These relate to a single component in an entire system. An example of such a twin could be that of a modulator or a laser.

Asset twins:
These represent the twin of a subsystem where two or more components work together. An example is an optical transmitter comprised of different components such as a laser, modulator, bias control and so on.

System (or unit) twins:
These represent a higher level of abstraction than assets. A system twin captures how different assets work together as part of a broader system. This could be a lightpath within an optical network.

Process twins:
Process twins capture the digital environment of a whole object, providing insight into how its various components, assets, and units work together. In an optical communications environment, this could capture the routing, modulation and spectrum assignment, thereby capturing the whole physical optical network from the perspective of the IP layer.

C. Requirements for a Digital Twin

To understand the requirements for the digital twin for any optical communication systems or components, we recall the definition of digital twins from Grieves [14] and refer to Fig. 16. It consists of three elements: real space, virtual space(s),

and a linking mechanism, referred to as data, and information/ process connection between real space and virtual space.

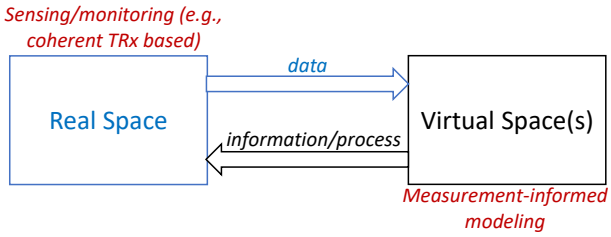

Fig. 16. Elements of the digital twin: real system, virtual system, the connections of data and information that connect the real and virtual system. The measurement data is captured from the real system while modeling of the real system can be done using the data in the virtual system to generate information for the real system.

The key is the linking mechanism that facilitates the automatic data flow from the physical object to the digital object and vice versa. Therefore, in practice, we need real-time, continuous measurements to be taken of the physical object. Lends itself to measurements, for example, that can be deduced from transceivers carrying live traffic for information to flow from the physical object to the digital object.

It also requires reliable measurement-informed modeling in the digital object and any changes there need to be reflected in the physical object. Note that digital objects will generate some variables as controllable, for example, modulation format, launch power, amplifier gain, etc.; others will not be such as fiber attenuation, dispersion, Raman gain profile of the fiber, etc.

D. Benefits of Using Digital Twin

There are several benefits of using digital twins for optical fiber communication systems ranging from the design and operational stages to forecasting. At the design stage, a digital twin allows testing and validation of the systems before deployment.

When used operationally, it facilitates the detection of any anomaly in the system. Digital twins operate in parallel with the real systems and identify operational behavior that deviates from the expected. An example of this could be the soft-failure identification of optical networks. Also, it enables operational optimization by providing necessary information on operational variables to get the best performance. Launch power optimization is an example of such a benefit.

Ultimately, a digital twin can be used to determine the remaining useful life of an asset and therefore predict the optimal time for servicing or replacement.

V. Recent Works on Digital Twins For Optical Fiber Communications

The initial use of digital twins was back in 1970 when NASA used mirrored systems on earth to rescue the stricken Apollo 13 space mission [102]. The concept of digital twins was proposed in 2003, however, the progress of the field was slow and was limited to manufacturing and industrial applications [103]. The growing stage of digital twins is only around in the last decade with widespread application in various areas including healthcare, manufacturing and process technologies, energy, smart cities, transportation, meteorology and environment, education, business and so on [92, 104].

The research of digital twins for optical communications has just started in the last few years; to the best of our knowledge, the first paper appeared in 2020 [105]. The authors proposed deep reinforcement learning-based digital twins for programmable optical transceivers (POT) modeling and controlling. The proposed twin could provide control information for the POT such as symbol rate, modulation format and FEC based on the real-time monitored data from an optical network. A similar approach was also described in [106].

Digital twining for soft-failure prediction, localization, and identification for optical networks was investigated in several publications. In [17], a digital twin framework was proposed to build the intelligent equipment fault management model, flexible hardware configuration model (controlling for POT), and transmission simulation model based on deep learning. In [107], a digital twin optical network (DTON) composed of four key elements: a data collector, data repository, service mapping models and digital twin entity manager was deployed and tested. The digital twins for soft failure detection and their severity estimation were investigated in [108, 109] using an NN-based model from constellation analysis (in the time domain) and an analytical model for spectrum evolution (in the frequency domain). An NN-based soft-failure location was demonstrated in [110] using principal component analysis. The combination of field data and synthetic data generated in a digital network twin was used for the training of such NN.

Digital twins for QoT estimation and prediction of optical networks were demonstrated in [18]. To enhance the estimation performance, input parameter refinement such as lumped (connectors) losses and amplifier gain spectra were taken into consideration. For prediction improvement, instead of static gain spectra of EDFA, an ML-based EDFA model accounting for the loading dependence was utilized. A cyber-physical system prototype including a digital twin for intelligent optical networks was outlined in [111] and as a use case, transmission performance prediction was demonstrated.

Digital twins not only allow QoT prediction but also enable launch power optimization in a multi-span transmission system. In [112], in the digital twin model, an NN was trained for a power evolution prediction for a multi-span link without any gain-flattering filter and then the trained NN was used in an autoencoder-based optimizer to obtain the optimized link input power spectrum. A similar approach was adopted in [19], where the NN was trained with SNR instead of power spectral density. The auto-encoder provides the optimized SNR and corresponding launch power profile. In [113], a physical layer model which is updated during the optimization process was used as a digital twin. As a study case, dynamic launch power optimization while the network in operation was demonstrated. Another SNR-optimization-based digital twin was created using a network automation framework, named AI-Light demonstrating the capability of optical channel power optimization [22]. A digital twin model for a multi-node WDM system utilizing only a single access point was experimentally demonstrated in [114] for prediction and

Table 1.: Summary of literatures using digital twins application in optical communication systems

Application(s)	Methodology used	References
Programmable optical transceivers	Deep reinforcement learning	[105], [106], [17]
Soft-failure prediction, localization and identification	Deep learning DTON framework Time- and frequency domain analysis Neural network	[17] [107] [108] [109] [110]
QoT estimation and prediction	ML-based EDFA modeling A cyber physical system prototype	[18] [111]
Transmit power profile optimization	Neural network and autoencoder ML-enhanced physical layer model AI-Light: a SDN framework Combined physics and ML based EDFA modeling	[112], [19] [113] [22] [114]
Physical layer modeling	GNPy- using GN model OCATA- using deep neural network Neural network	[115], [116], [20] [21] [117]
Coherent optical components	Complex-valued Volterra system identification	[118]
Network card failure identification and localization, and remote collaboration	Graph neural network and augmented-reality (AR)	[119]

optimization of the transmit power profile of each link in the network.

An open-source project, GNPy based on the GN model, was proposed as a network physical layer digital twin for open and disaggregated optical networks [115] [116]. Recently such an approach was experimentally tested on a network with a triangular topology that consists of multi-vendor open equipment [20]. A deep learning-based digital twin in the optical time domain, named OCATA was proposed in [21]. The lightpath of the network was realized using cascaded deep NN (DNN) for link and node. A digital twin of the unrepeated line was demonstrated using NN-based models of the remote optically pumped amplifier and Raman amplification [117].

Component-wise digital twin such coherent optical component (*e.g.* optical I/Q modulator) was investigated in [118]. The nonlinear response of the component was approximated with a complex-valued Volterra system identification method with a widely nonlinear phase retrieval from a direct-detection system.

Recently, an optical network digital twin using an ML-based model of both physical network elements as well as the operating environment has been introduced [119]. Using the interaction in a virtual environment utilizing augmented reality (AR), indoor navigation, network card failure identification and localization, and interactive remote collaboration over an 86-km optical link were demonstrated using the proposed digital twin.

A summary of digital twins-related literature with potential applications and key methodology is presented in Table 1.

As of the standardization effort, the Internet Engineering Task Force (IETF) agreed on the concept and reference architecture of digital twin networks as available in a published draft [120]. The proposed architecture consists of three layers: the real network, the digital twin network and an application layer that uses the digital twin. The IETF also published a draft for digital twins specific for packet and optical networks called performance-oriented digital twin (PODT) [121]. Two types of PODT are discussed. The first one is referred to as a network performance digital twin (NPDT) that produces performance estimates for a packet network and the other one is an optical performance digital twin (OPDT) that produces transmission performance estimates for an optical network.

VI. Open Challenges

Digital twins have only just started to emerge for optical fiber communication systems and thus there are still many open research challenges.

The most important challenge is to have measurement-based physical layer models that can continually update based on measurements and these models should be interpretable so that the operators have the confidence to use them. Hybrid analysis and modeling is promising in this respect, which is also a new emerging field for digital twins. Such modeling for the physical layer of optical networks will be a key task to solve. The modeling of physical layer components for open and disaggregated networks is particularly challenging as the components of the network are from multiple vendors and thus might have different characteristics.

Continual updating of models needs some careful consideration. It is important to take the uncertainty of measurements into account. However, from a complex systems perspective, the rare extreme events might be more

critical to capture. Also, as the physical system ages with time, proving corresponding changes in the model is difficult.

Another key challenge is to update multi-scale physics-based models for digital twins to merge component twins, asset twins, unit twins and process twins.

Telemetry is another important component of digital twins. Coherent transceiver-based telemetry is promising as outlined in this paper. However, additional optical, electrical or digital domain telemetry might be required especially for component or asset-based digital twinning. An efficient way for data collection. storage, access, process and communication with low latency needs to be ensured. Data fusion may be required for refining measured data and relaxing the data communication and storage requirements. Also, the low availability of field data from large-scale optical networks makes it challenging to link academic results with real-world practical applications.

Extended reality (immersive technologies like augmented reality (AR), virtual reality (VR) and mixed reality (MR)) can merge the physical and virtual world. Thus, utilizing the capabilities of extended reality for digital twins needs to be explored to allow the users to have close interaction with the digital representation of optical communication assets.

VIII. Conclusion

The capabilities of sensing the optical infrastructure by digital coherent receivers enable the generation of measurement data for physical layer modeling. In addition, the advancement of a hybrid approach of physics and data-driven modeling forms a solid basis for digital twins. Though there are still many challenges that need to be addressed, it is expected that, as the research progresses, digital twins will open a new avenue for optical network design and management in the near future.

References

[1] H. -M. Chin, K. Shi, R. Maher, M. Paskov, B. Thomsen and S. J. Savory, "Fast optical spectrum estimation using a digital coherent receiver," in *Eur. Conf. Opt. Commun. (ECOC)*, p. P3.23, 2013.

[2] I. Fatadin, Seb J. Savory and D. Ives, "Compensation of quadrature imbalance in an optical QPSK coherent receiver," *IEEE Photon. Technol. Lett.,* vol. 20, no. 20, pp. 1733-1735, 2008.

[3] Q. Sui, A. P. T. Lau and C. Lu, "Fast and robust blind chromatic dispersion estimation using auto-correlation of signal power waveform for digital coherent systems," *J. Lightw. Technol.,* vol. 31, no. 2, pp. 306-312, 2013.

[4] J. C. Geyer et al., "Channel parameter estimation for polarization diverse coherent receives," *IEEE Photon. Technol. Lett. ,* vol. 20, no. 10, p. 776–778, 2008.

[5] R. Rios-Müller, J. Renaudier, and G. Charlet, "Blind receiver skew compensation and estimation for long-haul non-dispersion managed systems using adaptive equalizer," *J. Lightw. Technol.,* vol. 33, no. 7, pp. 1315-1318, 2016.

[6] C. R. S. Fludger and T. Kupfer, "Transmitter impairment mitigation and monitoring for high baud-rate, high order modulation systems," in *Eur. Conf. Opt. Commun. (ECOC)*, p. Tu.2.A.2, 2016.

[7] F. J. Vaquero-Caballero, D. J. Ives and S. J. Savory, "Transceiver noise characterization based on perturbations," *J. Lightw. Technol.,* vol. 39, no. 18, pp. 5799-5804, 2021.

[8] D. J. Ives, B. C. Thomsen, R. Maher and S. J. Savory, "Estimating OSNR of equalised QPSK signals," *Opt. Exp.,* vol. 19, no. 26, pp. B661-B666, 2011.

[9] R. Schmogrow et al., "Error vector magnitude as a performance measure for advanced modulation formats," *IEEE Photon. Technol. Lett.,* vol. 24, no. 1, pp. 61-63, 2012.

[10] T. Tanimura, K. Tajima, S. Yoshida, S. Oda and T. Hoshida, "Experimental demonstration of a coherent receiver that visualizes longitudinal signal power profile over multiple spans out of its incoming signal," in *Eur. Conf. Opt. Commun. (ECOC)*, p. PD 3.4, 2019.

[11] A. May et al., "Longitudinal power monitoring over a deployed 10,000-km link for submarine systems," in *Opt. Fib. Commun. Conf. (OFC)*, p. Tu2G.3, 2023.

[12] A. Wunderlich, K. Booth and E. Santi, "Hybrid analytical and data-driven modeling techniques for digital twin applications," in *IEEE Electric Ship Technologies Symposium (ESTS)*, pp. 1-7, 2021.

[13] S. S. Blakseth, A. Rasheed, T. Kvamsdal, O. San,, "Combining physics-based and data-driven techniques for reliable hybrid analysis and modeling using the corrective source term approach," *App. Soft Comput.,* vol. 128, p. 109533, 2022.

[14] M. W. Grieves, "Product lifecycle management: the new paradigm for enterprises," *Int. J. Product Development,* vol. 2, no. 1/2, pp. 71-84, 2005.

[15] Q. Zhuge et al., "Building a digital twin for intelligent optical networks [Invited Tutorial]," *J. Opt. Commun. Net.,* vol. 15, no. 8, pp. C242-C262, 2023.

[16] D. A. A. Mello, K. S. Mayer, A. F. Escallón-Portilla, D. S. Arantes, R. P. Pinto and C. E. Rothenberg, "When digital twins meet optical networks operations," in *Opt. Fib. Commun. Conf. (OFC)*, p. W4A.3, 2023.

[17] D. Wang et al., "The role of digital twin in optical communication: fault management, hardware configuration, and transmission simulation," *IEEE Commun. Mag.,* vol. 59, no. 1, pp. 133-139, 2021.

[18] N. Morette, H. Hafermann, Y. Frignac and Y. Pointurier, "Machine learning enhancement of a digital twin for wavelength division multiplexing network performance prediction leveraging quality of transmission parameter refinement," *J. Opt. Commun. Net.,* vol. 15, no. 6, pp. 333-343, 2023.

[19] X. Pang et al., "Digital twin-assisted optical power allocation for flexible and customizable SNR optimization," in *Opt. Fib. Commun. Conf. (OFC)*, p. W4I.4, 2022.

[20] G. Borraccini et al., "Disaggregated optical network orchestration based on the physical layer digital twin," in *Opt. Fib. Commun. Conf. (OFC)*, p. Tu3D.4, 2023.

[21] D. Sequeira, M. Ruiz, N. Costa, A. Napoli, J. Pedro and L. Velasco,, "OCATA: a deep-learning-based digital twin for the optical time domain," *J. Opt. Commun. Netw.*, vol. 15, no. 2, pp. 87-97, 2023.

[22] A. Ferrari et al., "Demonstration of AI-light: an automation framework to optimize the channel powers leveraging a digital twin," in *Opt. Fib. Commun. Conf. (OFC)*, p. M3Z.14, 2022.

[23] Seb J. Savory, "Digital twins and measurement informed physical layer models [Invited Tutorial]," in *Opt. Fib. Commun. Conf. (OFC)*, p. M2F.1, 2023.

[24] Q. Zhuge, "AI-driven Digital Twin for Optical Networks," in *Eur. Conf. Opt. Commun. (ECOC)*, p. Mo3A.1, 2022.

[25] K. Kikuchi, "Fundamentals of coherent optical fiber communications," *J. Lightw. Technol.*, vol. 34, no. 1, pp. 157-179, 2016.

[26] M. S. Faruk and Seb J. Savory, "Digital signal processing for coherent transceivers employing multilevel formats," *J. Lightw. Technol.*, vol. 35, no. 5, pp. 1125-1141, 2017.

[27] H. -M. Chin, "Design of next generation optical transmission systems," PhD thesis, UCL, UK, 2016.

[28] C. Delezoide, P. Layec and S. Bigo, "Automated alignment between channel and filter cascade," in *Opt. Fib. Commun. Conf. (OFC)*, p. Th2A.48, 2019.

[29] K. Sun et al., "Digital residual spectrum-based generalized soft failure detection and identification in optical networks," *IEEE Tran. Commun.*, vol. 71, no. 1, pp. 324-338, 2023.

[30] M. Dallaglio et al., "Demonstration of a SDN-based spectrum monitoring of elastic optical networks," in *Opt. Fib. Commun. Conf. (OFC)*, p. Tu3L.5, 2017.

[31] Seb J. Savory, "Digital filters for coherent optical receivers," *Opt. Exp.*, vol. 16, no. 2, pp. 804-817, 2008.

[32] M. Kuschnerov, F. N. Hauske, K. Piyawanno, B. Spinnler, A. Napoli, and B. Lankl, B, "Adaptive chromatic dispersion equalization for non-dispersion managed coherent systems," in *Opt. Fiber Commun. Conf. (OFC)*, OMT1, 2009.

[33] C. Xie, "Chromatic dispersion estimation for single-carrier coherent optical communications," *IEEE Photon. Technol. Lett.* , vol. 25, no. 10, p. 992–995, 2013.

[34] F. N. Hauske, C. Xie, Z. Zhang, C. Li, L. Li, and Q. Xiong, "Frequency domain chromatic dispersion estimation," in *Opt. Fiber Commun. Conf. (OFC)*, p. JThA11, 2010.

[35] F. C. Pereira, V. N. Rozental, M. Camera, G. Bruno and D. A. A. Mello, "Experimental analysis of the power auto-correlation-based chromatic dispersion estimation method," *IEEE Photon. J.*, vol. 5, no. 4, p. 7901608, 2013.

[36] M. S. Faruk, Y. Mori, C. Zhang, K. Igarashi, and K. Kikuchi, "Multi-impairment monitoring from adaptive finite-impulse-response filters in a digital coherent receiver," *Opt. Exp.*, vol. 18, no. 26, pp. 26929-26936, 2010.

[37] F. N. Hauske, M. Kuschnerov, B. Spinnler, and B. Lankl, "Optical performance monitoring in digital coherent receivers," *J. Lightw. Technol.*, vol. 27, no. 26, p. 3623–3631, 2009.

[38] J. P. Gordon and H. Kogelnik, "PMD fundamentals: Polarization mode dispersion in optical fibers," *Proceedings of the National Academy of Sciences*, vol. 97, no. 9, pp. 4541-4550, 2000.

[39] M. Mazur et al., "Continuous fiber sensing over field-deployed metro link using real-time coherent transceiver and DAS," in *Eur. Conf. Opt. Commun. (ECOC)*, p. Mo4A.2, 2022.

[40] A. Mecozzi et al., "Use of optical coherent detection for environmental sensing," *J. Lightw. Technol.*, no. early access, 2023.

[41] F. Boitier et al., "Proactive fiber damage detection in real-time coherent receiver," in *in Eur. Conf. Opt. Commun. (ECOC)*, p. Th.2.F.1, 2017.

[42] Z. Zhan et al., "Optical polarization–based seismic and water wave sensing on transoceanic cables," *Science*, vol. 371, pp. 931-936, 2021.

[43] R. -J. Essiambre, G. Kramer, P. J. Winzer, G. J. Foschini and B. Goebel, "Capacity limits of optical fiber networks," *J. Lightw. Technol.*, vol. 28, no. 4, pp. 662-701, 2010.

[44] P. Ramantanis, C. Delezoide, P. Layec and S. Bigo, "Uncertainty aware real-time performance monitoring for elastic optical networks," in *Eur. Conf. Opt. Commun. (ECOC)* , pp. 1-4, 2021.

[45] E. R. Hartling et al., "Subsea Open Cables: A Practical Perspective on the Guidelines and Gotchas," in *Proc SubOptic*, 2019.

[46] M. S. Faruk and K. Kikuchi, "Monitoring of optical signal-to-noise ratio using statistical moments of adaptive-equalizer output in coherent optical receivers," in *Opto-Electron. and Commun. Conf. (OECC)*, p. 233-234, 2011.

[47] M. S. Faruk, Y. Mori and K. Kikuchi, "In-band estimation of optical signal-to-noise ratio from equalized signals in digital coherent receivers," *IEEE Photon. J.*, vol. 6, no. 1, p. 7800109, 2014.

[48] C. Zhu et al., "Statistical moments-based OSNR monitoring for coherent optical systems," *Opt. Exp.*,

vol. 20, no. 16, p. 17711–17721, 2012.

[49] Y. Ma, M. Gao, L. Wang, Y. Sha, W. Shao and G. Shen, "Accuracy enhancement of moments-based OSNR monitoring in QAM coherent optical communication," *IEEE Commun. Lett.*, vol. 24, no. 4, pp. 821-824, 2020.

[50] H. A. Mahmoud and H. Arslan, "Error vector magnitude to SNR conversion for nondata-aided receivers," *IEEE Trans. Wireless Commun.*, vol. 8, no. 5, pp. 2694-2704, 2009.

[51] R. Schmogrow et al., "Corrections to “Error vector magnitude as a performance measure for advanced modulation formats” [Jan 1, 2012 61-63]," *IEEE Photon. Technol. Lett.*, vol. 24, no. 23, pp. 2198-2198, 2012.

[52] C. Delezoide, P. Ramantanis and P. Layec, "On the performance prediction of optical transmission systems in presence of filtering," in *19th International Conference on Transparent Optical Networks (ICTON)*, p. We.B1.1, 2017.

[53] C. Delezoide, P. Ramantanis and P. Layec, "Weighted filter penalty prediction for QoT estimation," in *Opt. Fib. Commun. Conf. (OFC)*, p. W2A.56, 2018.

[54] T. Duthel, C. R. S. Fludger, J. Geyer and C. Schulien, "Impact of polarisation dependent loss on coherent POLMUX-NRZ-DQPSK," in *Opt. Fib. Commun. Conf. (OFC)*, p. OThU5, 2008.

[55] C. Delezoide, H. Akbari, P. Ramantanis, F. Boitier and P. Layec,, "Automated mitigation of quality of transmission fluctuations induced by PDL anomalies," in *Int. Conf. Opt. Net. Design and Modeling (ONDM)*, pp. 1-3 , 2023.

[56] P. K. Vitthaladevuni, M. -S. Alouini and J. C. Kieffer, "Exact BER computation for cross QAM constellations," *IEEE Trans. Wirel. Commun.*, vol. 4, no. 6, pp. 3039-3050, 2005.

[57] A. D. Shiner, "Neural network training for OSNR estimation from prototype to product," in *Opt. Fib. Commun. Conf. (OFC)*, p. M4E.2, 2020.

[58] F. J. Vaquero-Caballero, "Noise metrology in optical communication systems," PhD dissertation, University of Cambridge, 2021.

[59] G. P. Awgarwal, Fiber-optic communication systems, John Wiley & Sons, 2012.

[60] P. Poggiolini, G. Bosco, A. Carena, V. Curri, Y. Jiang and F. Forghieri, "The GN-model of fiber non-linear propagation and its applications," *J. Lightw. Technol.*, vol. 32, no. 4, p. 694–721, 2014.

[61] L. Berg, "Demystifying transceiver and line characterization metrics," in *Opt. Fib. Commun. Conf. (OFC)*, p. W4H.3, 2019.

[62] H. -M. Chin et al., "Probabilistic design of optical transmission systems," *J. Lightw. Technol.*, vol. 35, no. 4, pp. 931-940, 2017.

[63] D. J. Ives, H. -M. Chin, F. J. V. Caballero and S. J. Savory, "Single channel probe utilizing the EGN model to estimate link parameters for network abstraction," in *Eur. Conf. Opt. Commun. (ECOC)* , p. P2.SC6.13, 2017.

[64] A. Carena et al., "EGN model of non-linear fiber propagation," *Opt. Exp.*, vol. 22, no. 13, pp. 16335-16362, 2014.

[65] F. J. Vaquero-Caballero, D. J. Ives, C. Laperle, D. Charlton, Q. Zhuge, M. O’Sullivan, and Seb J. Savory, "Machine learning based linear and nonlinear noise estimation," *J. Opt. Commun. Netw.*, vol. 10, no. 10, pp. D42-D51, 2018.

[66] Z. Dong, A. P. T. Lau, and C. Lu, "OSNR monitoring for QPSK and 16-QAM systems in presence of fiber nonlinearities for digital coherent receivers," *Opt. Exp.*, vol. 20, no. 17, pp. 19520-19534, 2012.

[67] Z. Jiang et al., "Progresses of pilot tone based optical performance monitoring in coherent systems," *J. Lightw. Technol.*, vol. 40, no. 10, pp. 3128-3136, 2022.

[68] A. S. Kashi et al., "Fiber nonlinear noise-to-signal ratio monitoring using artificial neural networks," in *Eur. Conf. Opt. Commun. (ECOC)*, p. M.2.F.2, 2017.

[69] Q. Zhuge et al., "Application of machine learning in fiber nonlinearity modeling and monitoring for elastic optical networks," *J. Lightw. Technol.*, vol. 37, no. 13, pp. 3055-3063, 2019.

[70] T. Sasai, M. Nakamura, E. Yamazaki, S. Yamamoto, H. Nishizawa and Y. Kisaka, "Digital longitudinal monitoring of optical fiber communication link," *J. Lightw. Technol.*, vol. 40, no. 8, pp. 2390-2408, 2022.

[71] A. D. Shiner, A. Borowiec, M. Reimer, D. Charlton and M. O'Sullivan, "Nonlinear spatially resolved interferometer for distance resolved power and gain tilt measurement," in *Eur. Conf. Opt. Commun. (ECOC)*, p. 1-3, 2016.

[72] T. Tanimura, S. Yoshida, K. Tajima, S. Oda and T. Hoshida, "Fiber-longitudinal anomaly position identification over multi-span transmission link out of receiver-end signals," *J. Lightw. Technol.*, vol. 38, no. 9, pp. 2726-2733, 2020.

[73] C. Hahn, J. Chang and Z. Jiang, "Localization of reflection induced multi-path-interference over multi-span transmission link by receiver-side digital signal processing," in *Opt. Fib. Commun. Conf. (OFC)*, p. Th1C.3, 2022.

[74] S. Gleb, P. Konstantin, J. Luo and B. Zheng, "Fiber link anomaly detection and estimation based on signal nonlinearity," in *Eur. Conf. Opt. Commun. (ECOC)* , p. Tu2C2.5, 2021.

[75] I. Kim, O. Vassilieva, R. Shinzaki, M. Eto, S. Oda and P. Palacharla, "Robust longitudinal power profile estimation in optical networks using MMSE with complex scaling factor," in *Opt. Fiber Commun. Conf. [OFC]*, p. W4H.6, 2023.

[76] M. Sena et al., "DSP-based link tomography for amplifier gain estimation and anomaly detection in C+L-band systems," *J. Lightw. Technol.*, vol. 40, no. 11, pp. 3395-3405, 2022.

[77] T. Sasai, M. Nakamura, T. Kobayashi, H. Kawakami, E. Yamazaki and Y. Kisaka, "Revealing Raman-amplified power profile and Raman gain spectra with digital backpropagation," in *Opt. Fib. Commun. Conf. (OFC)*, p. M3I.5, 2021.

[78] M. Eto, K. Tajima, S. Yoshida, S. Oda and T. Hoshida, "Location-resolved PDL monitoring with Rx-side digital signal processing in multi-span optical transmission system," in *Opt. Fib. Commun. Conf. (OFC)*, p. Th1C.2, 2022.

[79] M. D. McKay, R. J. Beckman, W. J. Conover, "A comparison of three methods for selecting values of input variables in the analysis of output from a computer code," *Technometrics*, vol. 21, no. 2, pp. 239-245, 1979.

[80] P. Ramantanis, C. Delezoide, P. Layec and S. Bigo, "Revisiting the calculation of performance margins in monitoring-enabled optical networks," *J. Opt. Commun. Net.*, vol. 11, no. 10, pp. C67-C75, 2019.

[81] E. Seve, J. Pesic, C. Delezoide, S. Bigo and Y. Pointurier, "Learning process for reducing uncertainties on network parameters and design margins," *J. Opt. Commun. Net.*, vol. 10, no. 2, pp. A298-A306, 2018.

[82] J. W. Nevin, F. J. Vaquero-Caballero, D. J. Ives and S. J. Savory, "Physics-informed Gaussian process regression for optical fiber communication systems," *J. Lightw. Technol.*, vol. 39, no. 21, pp. 6833-6844, 2021.

[83] E. Seve et al., "Automated fiber type identification in SDN-enabled optical networks," *J. Lightw. Technol.*, vol. 37, no. 7, pp. 1724-1731, 2019.

[84] S. Oda et al., "A learning living network with open ROADMs," *J. Lightw. Technol.*, vol. 35, no. 8, pp. 1350-1356, 2017.

[85] M. Bouda et al., "Accurate prediction of quality of transmission with dynamically configurable optical impairment model," in *Opt. Fib. Commun. Conf. (OFC)*, p. Th1J.4, 2017.

[86] K. Christodoulopoulos et al., "Toward efficient, reliable, and autonomous optical networks: the ORCHESTRA solution [Invited]," *J. Opt. Commun. Net.*, vol. 11, no. 9, pp. C10-C24, 2019.

[87] C. Delezoide et al., "Marginless operation of optical networks," *J. Lightw. Technol.*, vol. 37, no. 7, pp. 1698-1705, 2019.

[88] O. Ayoub et al., "Towards explainable artificial intelligence in optical networks: the use case of lightpath QoT estimation," *J. Opt. Commun. Netw.*, vol. 15, no. 1, pp. A26-A38, 2022.

[89] G. E. Karniadakis, I. G. Kevrekidis, L. Lu, P. Perdikaris, S. Wang and L. Yang, "Physics-informed machine learning," *Nat. Rev. Phys.*, vol. 3, p. 422–440, 2021.

[90] A. Quarteroni and G. Rozza, Reduced order methods for modeling and computational reduction, New York: Springers, 2014.

[91] H. Robinson, S. Pawar, A. Rasheed and O. San, "Physics guided neural networks for modelling of non-linear dynamics," *Neur. Netw.*, vol. 152, p. 333–345, 2022.

[92] A. Rasheed, O. San and T. Kvamsdal, "Digital twin: values, challenges and enablers from a modeling perspective," *IEEE Access*, vol. 8, pp. 21980-22012, 2020.

[93] J. W. Nevin, S. Nallaperuma, N. A. Shevchenko, X. Li, M. S. Faruk, Seb J. Savory, "Machine learning for optical fiber communication systems: An introduction and overview," *APL photon.*, vol. 6, no. 12, p. 121101, 2021.

[94] D. Wang et al., "Applications of physics-informed neural network for optical fiber communications," *IEEE Commun. Mag.*, vol. 60, no. 9, pp. 32-37, 2022.

[95] X. Jiang, D. Wang, X. Chen and M. Zhang, "Physics-informed neural network for optical fiber parameter estimation from the nonlinear Schrödinger equation," *J. Lightwave Technol.*, vol. 40, no. 21, pp. 7095-7105, 2022.

[96] J. W. Nevin, S. Nallaperuma, Seb J. Savory, "Gaussian process-driven history matching for physical layer parameter estimation in optical fiber communication networks," *arXiv preprint*, p. arXiv:2202.11700, 2022.

[97] C. Meng, S. Seo, D. Cao, S. Griesemer, and Y. Liu, "When physics meets machine learning: A survey of physics-informed machine learning," *arXiv preprint*, p. arXiv:2203.16797, 2022.

[98] D. H. Gelernter, Mirror Worlds: or the day software puts the universe in a shoebox ...how it will happen and what it will mean, New York: Oxford University Press, 1991.

[99] M. Shafto et al., "Modeling, simulation, information technology & processing roadmap," *National Aeronautics and Space Administration*, vol. 32, pp. 1-38, 2012.

[100] "What is a digital twin?," IBM, [Online]. Available: https://www.ibm.com/topics/what-is-a-digital-twin. [Accessed June 2023].

[101] A. Fuller, Z. Fan, C. Day and C. Barlow, "Digital twin: enabling technologies, challenges and open research," *IEEE Access*, vol. 8, pp. 108952-108971, 2020.

[102] B. D. Allen, "Digital twins and living models at NASA," in *Digital Twin Summit*, 2021.

[103] F. Tao, H. Zhang, A. Liu and A. Y. C. Nee, "Digital twin in industry: State-of-the-art," *IEEE Trans.*

Industr. Inform., vol. 15, no. 4, pp. 2405-2415, 2019.

[104] F. Tao, B. Xiao, Q. Qi, J. Cheng, and P. Ji, "Digital twin modeling," *J. Manufact. Sys.,* vol. 64, pp. 372-389, 2022.

[105] J. Li, D. Wang, M. Zhang, and S. Cui, "Digital twin-enabled self-evolved optical transceiver using deep reinforcement learning," *Opt. Lett.,* vol. 45, no. 16, pp. 4654-4657, 2020.

[106] S. Cui, D. Wang , J. Li and M. Zhang, "Dynamic programmable optical transceiver configuration based on digital twin," *IEEE Commun. Lett.,* vol. 25, no. 1, pp. 205-208, 2021.

[107] R. Vilalta et al., "Architecture to deploy and operate a digital twin optical network," in *Opt. Fib. Commun. Conf. (OFC)*, p. W1F.4, 2022.

[108] M. Devigili, M. Ruiz, N. Costa, A. Napoli, J. Pedro and L. Velasco, "Dual time and frequency domain optical layer digital twin," in *Eur. Conf. Opt. Commun. (ECOC)*, p. Tu5.42., 2022.

[109] M. Devigili et al., "Degradation detection and severity estimation by exploiting an optical time and frequency digital twin," in *Opt. Fib. Commun. Conf. (OFC)*, p. W2A.18, 2023.

[110] K. S. Mayer et al., "Demonstration of ML-assisted soft-failure localization based on network digital twins," *J. Lightw. Technol.,* vol. 40, no. 14, pp. 4514-4520, 2022.

[111] L. Kuang, J. Wu and S. Yin, "Construct digital twin models in cyber space for physical objects of intelligent optical network," in *International Conferences on Internet of Things (iThings) and IEEE Green Computing & Communications (GreenCom) and IEEE Cyber, Physical & Social Computing (CPSCom) and IEEE Smart Data (SmartData) and IEEE Congress on Cybermatics (Cybermatics)*, p. 300-305, 2022.

[112] S. Li et al., "Digital twin-enabled power optimizer for multi-span transmission system using autoencoder," in *Opt. Fib. Commun. Conf. (OFC)*, p. M3H.1, 2021.

[113] A. Mahajan, K. Christodoulopoulos, R. Martinez, R. Munoz and S. Spadaro, "Quality of transmission estimator retraining for dynamic optimization in optical networks," *J. Opt. Commun. Net.,* vol. 13, no. 4, pp. B45-B59, 2021.

[114] R. T. Jones, K. R. H. Bottrill, N. Taengnoi, P. Petropoulos and M. P. Yankov, "Spectral power profile optimization of field-deployed wdm network by remote link modeling," in *Eur. Conf. Opt. Commun. (ECOC)* , p. We1A.4, 2022.

[115] J. Kundrát et al., "GNPy: lessons learned and future plans [Invited]," in *Eur. Conf. Opt. Commun. (ECOC)*, p. We3B.6, 2022.

[116] V. Curri, "GNPy model of the physical layer for open anddisaggregated optical networking [Invited]," *J. Opt. Commun. Net.,* vol. 14, no. 6, pp. C92-C104, 2022.

[117] A. Minakhmetov, B. Prieur, M. L. Monnier, D. Rouvillain and B. Lavigne, "Digital twin of unrepeatered line based on Raman and remote optically pumped amplifier machine learning models," in *Opt. Fib. Commun. Conf. (OFC)*, p. W4H.4, 2023.

[118] Y. Yoshida, "Widely nonlinear phase retrieval for direct detection-based digital twinning of coherent optical components," in *Opt. Fib. commun. conf. (OFC)*, p. We5.23, 2022.

[119] H. Chen et al., "Digital twin of a network and operating environment using augmented reality," *arXiv preprint*, p. arXiv:2303.15221, 2023.

[120] C. Zhou et al., "Digital twin network: concepts and reference architecture," draft, IETF, pp. 1-29, 2023.

[121] J. Paillisse et al., "Performance-oriented digital twins for packet and optical networks," draft, IETF, pp. 1-36, 2022.

Md Saifuddin Faruk (M'18, SM'23) received the B.Sc. and M.Sc. degrees in electrical and electronic engineering from KUET, Bangladesh in 2003 and BUET, Bangladesh in 2006, respectively and the Ph.D. degree in electrical engineering and information systems from the University of Tokyo, Japan in 2011. He is currently working as a senior research associate at the University of Cambridge. He also served as a faculty member in the department of electrical and electronic engineering of Dhaka University of Engineering and Technology (DUET), Bangladesh from 2004 to 2019. During 2015-2017, being on leave from DUET, he worked as Marie Curie Research Fellow in the University College London (UCL) and the University of Cambridge, UK. His current research interest includes DSP for coherent transceivers, high-speed optical access networks and machine learning applications for optical fiber communications.

Seb J. Savory (M'07, SM'11, F'17) received M.Eng., M.A., and Ph.D. degrees in engineering from the University of Cambridge and an M.Sc. (Maths) in mathematics from the Open University. His interest in optical fiber communication began in 1991, when he joined STL (subsequently Nortel) in Harlow, joining the labs full-time in 2000 after completing his PhD. In 2005, he moved to UCL where he held a Leverhulme Trust Early Career Fellowship from 2005 to 2007, before being appointed as a Lecturer (2007), Reader (2012) and Professor (2015). He returned to Cambridge in January 2016 as a University Lecturer, subsequently promoted to Professor of Optical Fibre Communication in October 2019. He currently serves as Vice President (Publications) for the IEEE Photonics Society. He is a Chartered Engineer and is a Fellow of the IEEE, IET, Optica/OSA, HEA and Churchill College, Cambridge.